Nanostructures

DOI: 10.1002/ange.201300285

Ultrathin Nanosheets of MAX Phases with Enhanced Thermal and Mechanical Properties in Polymeric Compositions: $Ti_3Si_{0.75}Al_{0.25}C_2$**

*Xiaodong Zhang, Jianguang Xu, Hui Wang, Jiajia Zhang, Hanbing Yan, Bicai Pan, Jingfang Zhou, and Yi Xie**

Since first reported, layered ternary carbides and nitrides named "MAX phases" from $M_{n+1}AX_n$ ($n=1$, 2 or 3) phases, where M is a transition metal, A is a group IIIA or IVA element, and X is carbon or nitrogen atoms, have attracted the attention of scientists and industry for their unique combination of metallic and ceramic properties.[1] For example, MAX phases show excellent resistance to oxidation, heat, and corrosion, high electrical conductivity, high strength and elastic modulus, and are easily produced, benefiting from their inherent lamellar structure with alternately arranged MX and A layers (Figure 1 a).[2–4] Currently, the study and application of MAX phases is still restricted to three-dimensional (3D) bulk samples. Nanosized materials, especially ultrathin two-dimensional (2D) nanosheets, show enhanced properties with respect to their corresponding bulk counterpart.[5–8] For example, free-standing graphene shows remarkable in-plane thermal conductivity and mechanical strength, up to about 3000 $W m^{-1} K^{-1}$ and 1060 GPa, respectively.[8,9] The thermal conductivity and mechanical strength of ultrathin boron nitride (BN) nanosheets are theoretically estimated as high as 2000 $W m^{-1} K^{-1}$ and 800 GPa,[10] respectively, which are much higher than the value of the corresponding bulk materials. Benefiting from these properties, graphene and BN nanosheets are considered to be promising fillers in polymeric composites, to improve their thermal and mechanical properties.[11–15] Accordingly, we anticipate enhanced properties of ultrathin nanosheets of MAX phases with respect to the bulk materials.

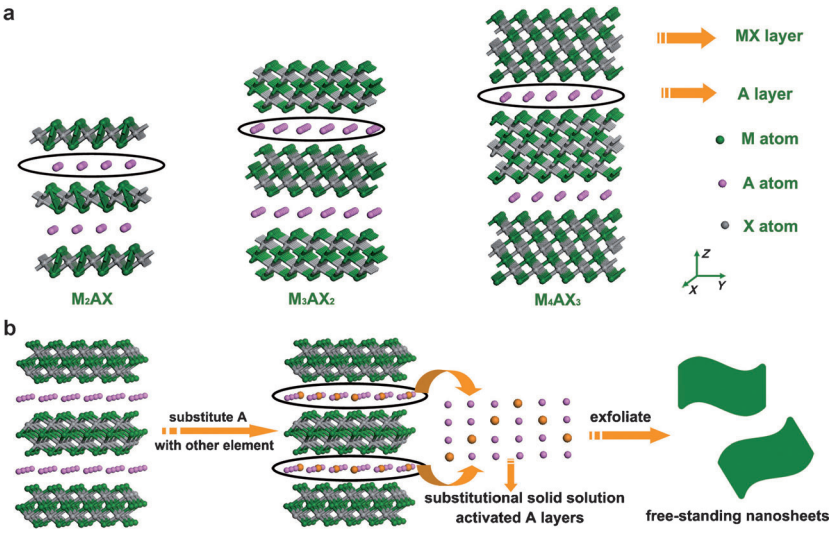

Figure 1. a) Crystal structure of 211, 312, and 413 MAX phases. b) Illustration of the substitutional solid solution based exfoliation process for the formation of free-standing nanosheets of MAX phases by activating the A layers.

However, in contrast to inorganic graphene analogues (IGAs), with a weak van der Walls force between the layers, the MAX phases possess relatively strong bonds between the MX and A layers, and it has not been possible for these materials to be exfoliated into ultrathin nanosheets using simple exfoliation processes.[16,17] Recently, Naguib et al. have reported the preparation of "MXenes" by extraction of the A layers from the MAX phases in a solution of hydrofluoric acid (HF),[16,17] and the as-prepared MXenes show novel electronic and magnetic properties.[18,19] However, it is only when the A layer is aluminum that the MAX phases can be etched with HF and exfoliated into MXenes and the use of HF in the etching process is dangerous and toxic, both of these conditions will undoubtly restrict the application of this

[*] X. D. Zhang,[+] H. Wang, J. J. Zhang, Prof. B. C. Pan, Prof. Y. Xie
Hefei National Laboratory for Physical Science at Microscale,
University of Science and Technology of China
Hefei, Anhui, 230026 (P. R. China)
E-mail: yxie@ustc.edu.cn
Prof. J. G. Xu,[+] H. B. Yan
Jiangsu Provincial Key Laboratory of Eco-Environmental Materials,
Yancheng Institute of Technology
Yancheng, Jiangsu, 224051 (P. R. China)
H. B. Yan
College of Electromechanical and Engineering
Hunan University of Science and Technology
Xiangtan, Hunan, 411201 (P. R. China)
Prof. J. F. Zhou
Ian Wark Research Institute, Mawson Lakes Campus
University of South Australia
South Australia 5095 (Australia)
[+] These authors contributed equally to this work.

[**] We thank the National Basic Research Program of China (2009CB939901), Chinese Academy of Science (XDB01020300), and National Natural Science Foundation of China (11079004 and 90922016) for financial support. MAX phases comes from $M_{n+1}AX_n$ ($n=1$, 2, or 3) phases, where M is a transition metal, A is a group IIIA or IVA element, and X is carbon or nitrogen atoms.
Supporting information for this article is available on the WWW under http://dx.doi.org/10.1002/anie.201300285.

method. In addition, because the A elements are missing in the as-prepared MXenes, they do not have the same intrinsic properties as MAX phases. There are more than 60 types of MAX phases, and it would be highly useful to develop a universal method for the preparation of nanosheets from such ternary compounds. Thus, developing a green, facile, and effective method for the preparation of the ultrathin nanosheets of MAX phases is urgently needed.

Although MAX phases are chemically stable, the A layers are more reactive than the MX layers. Therefore, if we further activate the A layers by substituting a portion of the A atoms with other elements, forming a substitutional solid solution, the as-doped MAX phases could be exfoliated by breaking the bonds between the A and MX layers (Figure 1b). According to the Hume–Rothery rules for the formation of stable substitutional solid solutions: first, the atomic radii of solute and solvent atoms must differ by no more than 15%; second, the crystal structure of the solute and solvent should match with each other; third, the solute and solvent atoms should have similar electronegativity. In MAX phases, there are pairs of materials that obey the basic rules described above, such as, Ti_2AlC and Ti_2GaC, V_2GaC and V_2GeC, Hf_2InC and Hf_2SnC, Ti_3AlC_2 and Ti_3SiC_2, Ti_4SiC_3 and Ti_4GeC_3, among others.[1] Benefiting from recent experimental progress on controlling the synthesis, a series of elementally doped MAX phases could be prepared for further study.

Herein, for the first time, we use an available substitutional solid solution based exfoliation process for the large-scale fabrication of ultrathin nanosheets of A-layer-activated MAX phases. In this study, taking Ti_3SiC_2 and Ti_3AlC_2 of the 312 MAX phase, we fabricated a series of doped phases, such as, $Ti_3Si_{0.75}Al_{0.25}C_2$ (TSAC) and $Ti_3Al_{0.9}Si_{0.1}C_2$ (TASC), using a modified high-temperature self-propagation synthesis (see the Supporting Information). Using TSAC as an example, we systematically studied the exfoliation process and potential use of this material as an effective filler in polymeric composites of the as-exfoliated nanosheets. The small amount of TiC in the as-prepared bulk TSAC was formed during the synthesis (Supporting Information, Figure S1), which is a common phenomenon for high-temperature self-propagation synthesis and can be easily removed by centrifugation of the suspension of TSAC nanosheets.

Our experiments show that the TSAC powder can be exfoliated into ultrathin nanosheets using several solvents; in comparison, pure Ti_3SiC_2 powder cannot be exfoliated into nanosheets in these same solvents (Figures S2,S6). In addition, the TASC powder can also be exfoliated into ultrathin nanosheets in various solvents to form a stable suspension (Figure S5), which indicates wide applicability of the substitutional solid solution based exfoliation method for the preparation of MAX phase nanosheets. In the absence of high-temperature treatment or a chemical reaction, the as-exfoliated nanosheets retain the same crystal structure and chemical stoichiometric ratio of the corresponding bulk materials and have the intrinsic properties of the MAX phases.

Figure 2a is a transmission electron microscopy (TEM) image of the as-exfoliated nanosheets, which shows the free-standing nanosheets with a range of diameters from 100 nm to 200 nm. The Tyndall effect in the suspension (Figure 2d) indicates the presence of highly monodisperse ultrathin TSAC nanosheets in *N*,*N*-dimethylformamide (DMF). A high-resolution TEM (HRTEM) image of a typical TSAC nanosheet and its corresponding selected area electron diffraction (SAED) pattern (Figure 2b) reveal the single-crystalline nature of the as-exfoliated nanosheet. The lattice fringes of 2.64 Å correspond to the {100} lattice plane of the TSAC crystal structure, indicating that the nanosheets have exposed the *XY*-plane and have been exfoliated along the Z-axis. Energy dispersive spectroscopy (EDS) analysis shows that the molar ratio between Si and Al atoms of the as-exfoliated TSAC nanosheets is about 3:1 (Figure 2c), which is consistent with the stoichiometric ratio of bulk TSAC powder. Tapping-mode atomic force microscopy (AFM) analysis (Figure 2e and f) shows that the thickness of the as-exfoliated TSAC nanosheets is only about 4 nm, which is the thickness of about two to three layers of the TSAC crystal.

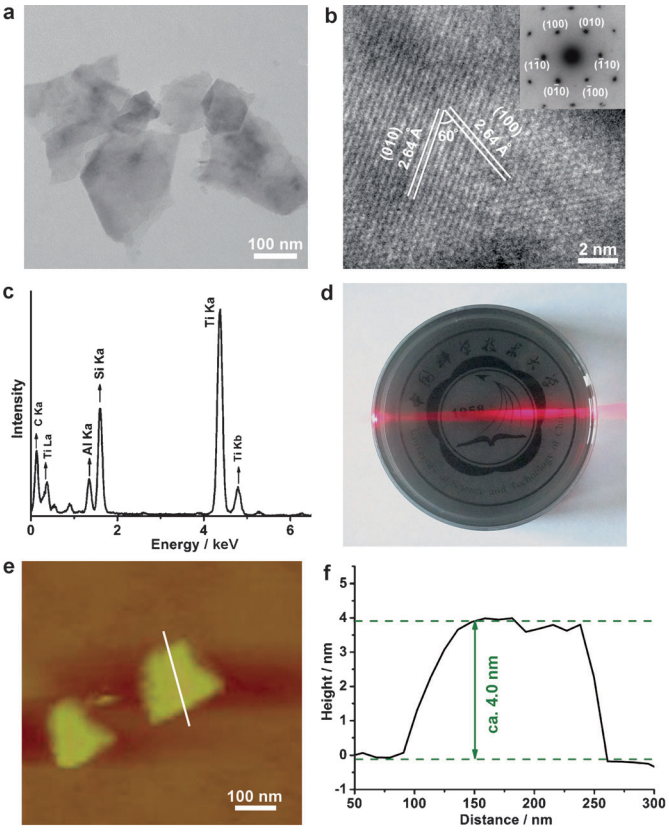

Figure 2. a) TEM image of TSAC nanosheets. b) HRTEM image of a typical TSAC nanosheet, inset: the corresponding SAED pattern. c) EDS pattern of TSAC nanosheet. d) Tyndall effect of TSAC nanosheets dispersed in DMF. e) AFM image of TSAC nanosheets and f) the corresponding height measurement.

Ultrathin 2D nanosheets should show enhanced intrinsic properties with respect to their bulk counterpart,[5–8] similar to graphene and BN nanosheets, we anticipated that the as-exfoliated TSAC nanosheets would have excellent thermal and mechanical properties. Herein, we carried out first-principle density-functional theory (DFT) calculations to study the electronic structure and Young's modulus of the bulk and single-layered nanosheets of TSAC.

The calculated density of states (DOS) of the bulk and single-layered nanosheets of TSAC are shown in Figure 3a. This analysis shows that both forms possess metallic characteristics, indicating that partial substitution of Si with Al atoms in the Ti_3SiC_2 crystal does not change its intrinsic

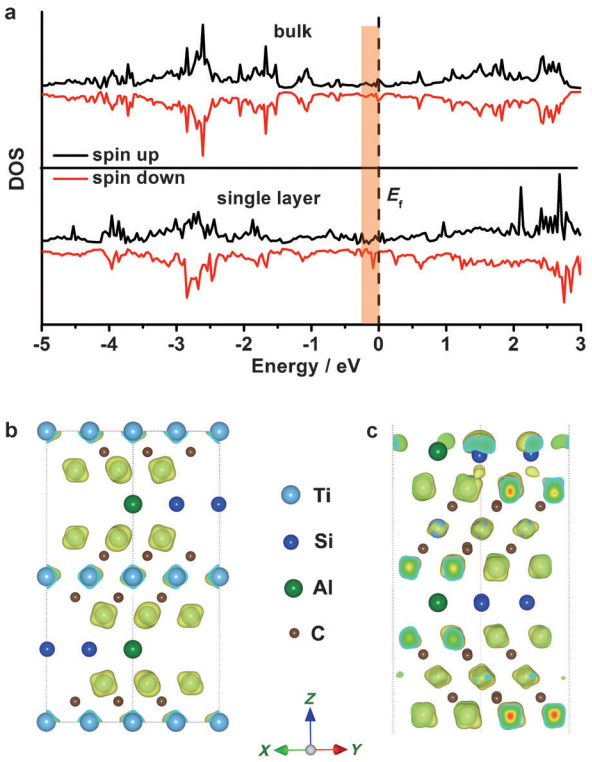

Figure 3. a) Calculated density of states (DOS) for bulk TSAC and single-layered TSAC nanosheets. The shaded part shows the occupied states of electrons with about 0.26 eV to Fermi level (E_f). b,c) Charge density wave of bulk TSAC and single-layered TSAC nanosheet at the edge of the Fermi level, respectively.

metallic properties. The number of electrons at the edge of the occupied state is crucial to the metallic property, therefore we studied TSAC in the area of $E_f - E \leq 10\,k_B\,T$, where k_B is the Boltzmann constant, T is the absolute temperature of 300 K, and $10\,k_B T$ is estimated to be about 0.26 eV, which is estimated to be about 3.76 electrons for bulk and 4.96 electrons for the nanosheets. These results indicate that the single-layered TSAC nanosheets possess more electrons than their corresponding bulk counterparts at the occupied states of about 0.26 eV to the Fermi level (the shadowed part of Figure 3a), which can also be clearly seen from the charge density wave of bulk and single-layered nanosheets of TSAC. Figure 3b is the wave function of bulk TSAC at the edge of the Fermi level, which is mainly contributed by the d orbital of titanium. However, the wave function of a single-layered TSAC nanosheet is mainly derived from the d orbital of titanium and the s and p orbitals of silicon (Figure 3c). The enhanced density of states of single-layered nanosheets with respect to the bulk counterpart can be ascribed to the presence of dangling silicon bonds during the exfoliation process and the increased contribution from the d orbital of titanium.

It is known that, for metals the thermal conductivity is mostly derived from the charge carrier; therefore, the more electrons that a material possesses the higher the thermal conductivity will be. The single-layered TSAC nanosheets should show enhanced thermal conductivity with respect to their corresponding bulk counterparts. In addition, the single-layered TSAC nanosheets also show enhanced mechanical properties, with an extremely high Young's modulus of about 404 GPa, comparable to the value of graphene and BN nanosheets.[6,7] However, the Young's modulus of bulk TSAC is theoretically estimated to be only about 98 GPa.

TSAC nanosheets could display the advantages of 2D crystal structures, and their excellent thermal and mechanical properties make them a promising candidate for applications in polymeric composites. By making a novel poly(methyl methacrylate) (PMMA)/TSAC nanosheet composite, we show that the TSAC nanosheets can significantly improve the heat tolerance of PMMA while the mechanical properties of the composite are simultaneously enhanced. Films of pure PMMA, PMMA/bulk TSAC, and PMMA/TSAC nanosheet composites with a thickness of about 50 μm were prepared for further study (see the Supporting Information). Both of the composite films and the pure PMMA film show transparent and flexible characteristics (Figure 4a,b). After embedding the as-exfoliated TSAC nanosheets or bulk TSAC powder in PMMA the transmission of light of the composite films was decreased but was still at a high level, up to 80%.

Differential scanning calorimetry (DSC) was carried out to study the glass-transition temperature (T_g) of the as-prepared films of PMMA and its composites. As estimated from the midpoint of the heat capacity peaks (Figure 4c), the T_g of the pure PMMA film was about 62.2°C, the PMMA/bulk TSAC film was 68.5°C, and the PMMA/TSAC nanosheets film was 73.0°C. The T_g of the PMMA/TSAC nanosheet film was about 10°C higher than pure PMMA and about 5°C higher than the PMMA/bulk TSAC film, indicating the mobility of the polymer chains can be effectively confined by the embedded TSAC nanosheets. Notably, the amount of TSAC in the composites is only about 0.3 wt%. For the ultrathin thickness of the as-exfoliated TSAC nanosheets, the surface area is higher than the bulk counterpart. Furthermore, the TSAC nanosheets have abundant dangling bonds at the surface resulting from the unsymmetrical break of the Ti-Si/Ti-Al bonds. Both of the these things promote the interfacial interaction between TSAC nanosheets and PMMA, which slows the relaxation dynamics of the PMMA chains, leading to an increase in the T_g and the configuration entropy of PMMA/TSAC nanosheet composite compared with pure PMMA and PMMA/bulk TSAC composite, as shown in the DSC curves of Figure 4c.[14] The T_g of the PMMA/TSAC nanosheet composite increases with the increasing of amount of TSAC nanosheets in the composite (Figure S8).

The slow relaxation dynamics of PMMA chains in the PMMA/TSAC composites can also be demonstrated by the thermal expansion of the as-prepared films. As shown in Figure 4d, the pure PMMA film possesses the highest thermal expansion, in comparison, the thermal expansion of the

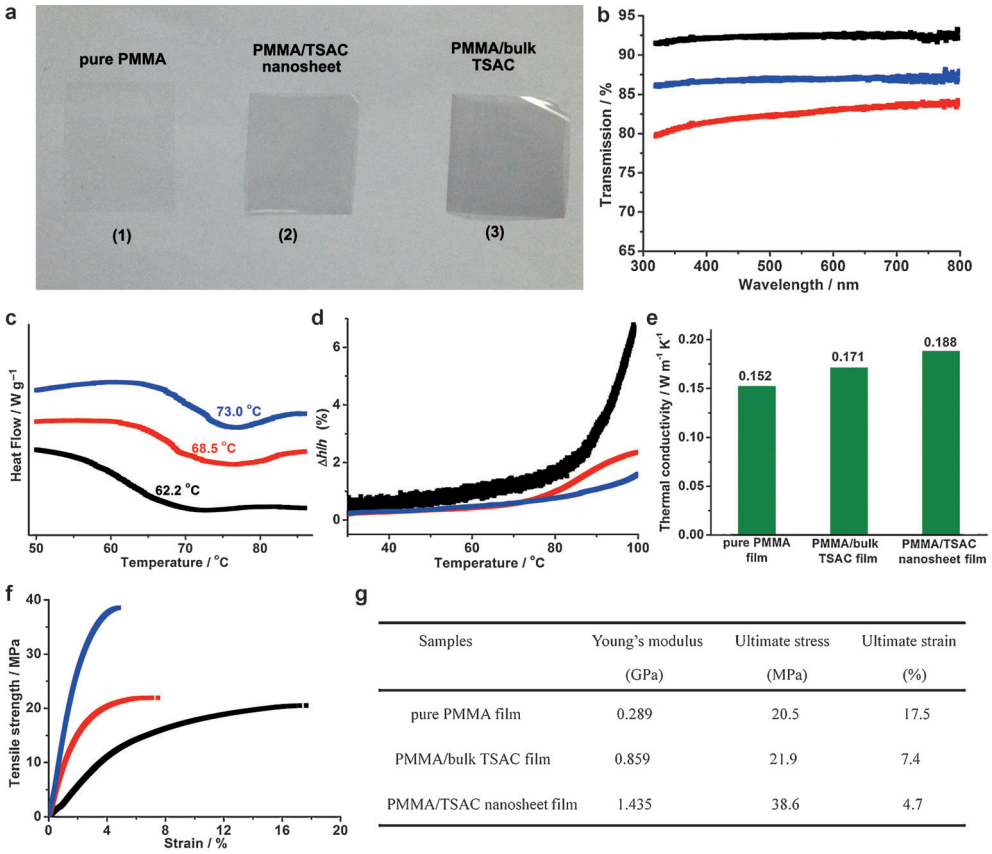

g

Samples	Young's modulus (GPa)	Ultimate stress (MPa)	Ultimate strain (%)
pure PMMA film	0.289	20.5	17.5
PMMA/bulk TSAC film	0.859	21.9	7.4
PMMA/TSAC nanosheet film	1.435	38.6	4.7

Figure 4. a) Photograph, b) UV/Vis transmittance spectra, c) DSC curves, d) thermal expansion curves, e) thermal conductivity, and f) tensile strength–strain curves of pure PMMA, PMMA/bulk TSAC film, and PMMA/TSAC nanosheets films. g) Summary of the mechanical properties of the films measured by tensile testing. For (b–d, f), black = pure PMMA film, red = PMMA/bulk TSAC composite film, blue = PMMA/TSAC nanosheet composite film

composite films were reduced by embedding TSAC in PMMA. The PMMA/bulk TSAC film and PMMA/TSAC nanosheet film show negligible thermal expansion below the T_g, however, both of them show a slight increase in thermal expansion above the T_g. The PMMA/bulk TSAC film shows nearly twofold higher expansion with respect to the PMMA/TSAC nanosheets film at 100 °C. These results indicate that the TSAC nanosheets are more effective at restricting the mobility of the polymer chains and tolerating heat. Because the TSAC nanosheets have more electrons than the bulk sample near the Fermi level, we would predict an excellent thermal conductivity of the PMMA/TSAC nanosheet composite compared with the pure PMMA and PMMA/bulk TSAC composite. The thermal conductivity of PMMA/TSAC nanosheets film was measured to be about 0.188 $W m^{-1} K^{-1}$, which is a 23 % and 10 % increase in the value with respect to pure PMMA (0.152 $W m^{-1} K^{-1}$) and PMMA/bulk TSAC composite (0.171 $W m^{-1} K^{-1}$), respectively, indicating that a small amount of TSAC nanosheets can greatly improve the thermal conductivity of PMMA (Figure 4e).

In addition to the improvement of thermal properties, the PMMA/TSAC nanosheet film also shows enhanced mechanical reinforcement. As shown in Figure 4f,g, the Young's modulus and ultimate tensile strength of the PMMA/TSAC nanosheets are about fivefold and twofold higher than that of the pure PMMA film, respectively, both of which are about twofold higher than that of the PMMA/bulk TSAC film. The improvement of the mechanical properties of the PMMA/TSAC nanosheet film indicates that the embedded TSAC nanosheets can effectively transfer the applied mechanical strength, owing to the interfacial interaction between the TSAC nanosheets and PMMA molecules. Embedding only 0.3 wt % of the as-exfoliated TSAC nanosheets in the PMMA gave a nearly fivefold and twofold increase in the Young's modulus and ultimate tensile strength, respectively, much higher than the well-known PMMA/BN nanosheet and PMMA/graphene composites at the same weight percent of nanosheet,[12–14] indicating the potential of applying TSAC nanosheets in polymer composites.

In conclusion, we have developed a substitutional solid solution based exfoliation method for the preparation of nanosheets of MAX phases by substituting a portion of A with other elements for the formation of a substitutional solid solution to activate the A layers for the first time, which was illustrated using TSAC nanosheets. Compared with the bulk counterpart, TSAC nanosheets were predicted to have enhanced thermal and mechanical properties, which makes them suitable for the use in polymeric composites. The as-prepared PMMA/TSAC nanosheet composite shows excellent thermal and mechanical properties, such as, improved T_g, thermal conductivity, Young's modulus, and decreased thermal expansion, with respect to pure PMMA and PMMA/bulk TSAC composite, benefiting from the effective interfacial interaction between the TSAC nanosheets and the PMMA polymer chains. The improvement of the thermal and mechanical properties of the new PMMA/TSAC nanosheet composite are comparable or superior to PMMA/BN nanosheet and PMMA/graphene composites with the same content of nanosheet. This makes the application of the TSAC nanosheets in polymer composites very promising.

Received: January 12, 2013
Published online: March 19, 2013

Keywords: MAX phases · mechanical properties · nanosheets · solid-phase synthesis · solid-state reactions

[1] P. Eklund, M. Beckers, U. Jansson, H. Högberg, L. Hultman, *Thin Solid Films* **2010**, *518*, 1851.
[2] X. H. Wang, Y. C. Zhou, *J. Mater. Sci. Technol.* **2010**, *26*, 385.
[3] M. W. Barsoum, M. Radovic, *Annu. Rev. Mater. Res.* **2011**, *41*, 195.
[4] R. Ahuja, O. Eriksson, J. M. Wills, B. Johansson, *Appl. Phys. Lett.* **2000**, *76*, 2226.
[5] Y. Sun, H. Cheng, S. Gao, Z. Sun, Q. Liu, Q. Liu, F. Lei, T. Yao, J. He, S. Wei, Y. Xie, *Angew. Chem.* **2012**, *124*, 8857; *Angew. Chem. Int. Ed.* **2012**, *51*, 8727.
[6] X. Zhang, X. Xie, H. Wang, J. Zhang, B. Pan, Y. Xie, *J. Am. Chem. Soc.* **2013**, *135*, 18.
[7] L. Lindsay, D. A. Broido, *Phys. Rev. B* **2011**, *84*, 155421.
[8] S. Chen, Q. Wu, C. Mishra, J. Kang, H. Zhang, K. Cho, W. Cai, A. A. Balandin, R. S. Ruoff, *Nat. Mater.* **2012**, *11*, 203.
[9] S. Stankovich, D. A. Dikin, G. H. B. Dommett, K. M. Kohlhaas, E. J. Zimney, E. A. Stach, R. D. Piner, S. T. Nguyen, R. S. Ruoff, *Nature* **2006**, *442*, 282.
[10] Y. Lin, J. W. Connell, *Nanoscale* **2012**, *4*, 6908.
[11] L. M. Veca, M. J. Meziani, W. Wang, X. Wang, F. Lu, P. Zhang, Y. Lin, R. Fee, J. W. Connell, Y.-P. Sun, *Adv. Mater.* **2009**, *21*, 2088.
[12] T. Ramanathan, A. A. Abdala, S. Stankovich, D. A. Dikin, M. Herrera Alonso, R. D. Piner, D. H. Adamson, H. C. Schniepp, X. Chen, R. S. Ruoff, S. T. Nguyen, I. A. Aksay, R. K. Prud' Homme, L. C. Brinson, *Nat. Nanotechnol.* **2008**, *3*, 327.
[13] G. Gonçalves, P. A. A. P. Marques, A. Barros-Timmons, I. Bdkin, M. K. Singh, N. Emami, J. Grácio, *J. Mater. Chem.* **2010**, *20*, 9927.
[14] C. Zhi, Y. Bando, C. Tang, H. Kuwahara, D. Golberg, *Adv. Mater.* **2009**, *21*, 2889.
[15] W.-L. Song, P. Wang, L. Cao, A. Anderson, M. J. Meziani, A. J. Farr, Y.-P. Sun, *Angew. Chem.* **2012**, *124*, 6604; *Angew. Chem. Int. Ed.* **2012**, *51*, 6498.
[16] M. Naguib, M. Kurtoglu, V. Presser, J. Lu, J. Niu, M. Heon, L. Hultman, Y. Gogotsi, M. W. Barsoum, *Adv. Mater.* **2011**, *23*, 4248.
[17] M. Naguib, O. Mashtalir, J. Carle, V. Presser, J. Lu, L. Hultman, Y. Gogotsi, M. W. Barsoum, *ACS Nano* **2012**, *6*, 1322.
[18] M. Khazaei, M. Arai, T. Sasaki, C.-Y. Chung, N. S. Venkataramanan, M. Estili, Y. Sakka, Y. Kawazoe, *Adv. Funct. Mater.* **2012**, DOI: 10.1002/adfm.201202502.
[19] Z. Zhang, X. Liu, B. I. Yakobson, W. Guo, *J. Am. Chem. Soc.* **2012**, *134*, 19326.

